Compressive Self-powering of Piezo-Floating-Gate Mechanical Impact Detectors

Pikul Sarkar and Shantanu Chakrabartty, *Senior Member, IEEE*

***Abstract*—This paper describes a novel compressive self-powering technique that significantly extends the powering and sensing range of our previously reported piezo-floating-gate (PFG) sensors for applications in mechanical impact monitoring. At the core of the proposed technique is a non-linear impedance circuit that dynamically loads the output of a piezoelectric transducer in a manner such that the sensor can be self-powered at low-levels of mechanical strain and yet is able to sense and detect large variations in strain-levels. The compressive approach requires precise programming of event detection thresholds and requires precise non-volatile event counting, both of which are achieved using variants of a linear floating-gate injector circuit. Measured results obtained from prototypes fabricated in a 0.5-μm standard CMOS process validate the proposed compressive powering and the proposed programming technique.**

***Index Terms*—Self-powered sensors, mechanical impact detection, strain, compressive powering, floating-gate transistor, piezoelectricity, structural health monitoring.**

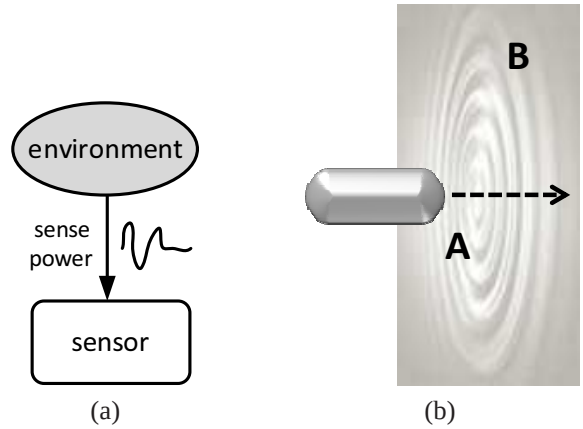

Fig. 1. (a) Operational power of a sensor harvested directly from the signal being sensed; (b)Bullet impact on an armor with sensors embedded at positions A and B.

I. Introduction

Self-powered sensing refers to an energy scavenging paradigm where the operational power of a sensor is harvested directly from the signal being sensed [1]. For example, a piezoelectric transducer could be used for sensing variations in mechanical strain and the energy in the strain variations could also be used for the computation and storage. As a result, the operation of the self-powered sensor can be asynchronous (shown in Fig. 1(a)) where events of interest can directly energize the computing and storage circuits. In this manner, the asynchronous sensor can continuously monitor for events of interest without experiencing any down-time [1], a feature that can not be guaranteed with conventional synchronous energy scavenging approaches [2], [3]. The event signatures can then be stored on a non-volatile memory and can be remotely retrieved at a later period of time. One possible application, where such a sensor could be used, is for the design of smart armors. This is illustrated in Fig. 1(b) where the mechanical impact of a bullet or an artillery energizes an array of embedded sensors which compute and store the strength and the signature of the impact. These data could then be used to prognosticate when and where the armor could potentially fatigue [4], [5].

This work is supported by research grants from the National Science Foundation (CAREER:0954752, AIR:1127606). Pikul Sarkar and Shantanu Chakrabartty are affiliated with the Department of Electrical & Computer Engineering, Michigan State University, East Lansing, Michigan 48824, USA. All correspondences regarding this paper should be addressed to Email: shantanu@egr.msu.edu.

One of challenges in designing self-powered sensors that can operate over a large sensing range is the *threshold effect*. The sensor electronics powered by the transducer typically requires a minimum voltage for start-up or to be energized. For instance, in the strain-powered sensor reported in [1], a minimum of 5V (at a load of 10MΩ) is required to activate the non-volatile storage functions. On the other hand, the upper limit on the magnitude of the sensor signal is determined by the breakdown voltages of active components on-chip or the threshold of the Zener protection diodes. For example, the maximum voltage of the sensor described in [1] is 9V which is determined by the reverse break-down voltage of the ESD diodes. Both the lower and upper threshold in the sensor signal severely limits the operating and sensing range of the sensor as shown in Fig. 2 (a). Assuming a sensor that is powered by a piezoelectric transducer, the lower voltage threshold V_{min} determines the minimum strain ε_{min} that needs to be applied before the sensor becomes operational, and the higher voltage threshold V_{max} determines the maximum strain-level that can be sensed ε_{max}. The effect remains unchanged if a high-gain (high mechanical-to-electrical conversion coefficient) single-crystal piezoelectric transducer (Piezo-A with range of A_1 to A_2) is used (as shown in Fig. 2(a)), which even though lowers the minimum strain-level required for powering the sensor but significantly reduces the maximum level of strain that can be sensed. For applications like the smart armor, as illustrated in Fig. 1(b), the *threshold effect* poses a significant problem. The velocity of a bullet impinging the armor could be as high as 854.35 m/s [6], [7], [8] (impact energy exceeding 100J) and depending on the placement of the sensor and the point of

impact, the mechanical strain could vary over several orders of magnitude. Likewise, if a low gain piezoelectric transducer (Piezo-B with range of B_1 to B_2) is used, the sensor could only be activated at relatively large strain-levels.

To alleviate the problems associated with the *threshold effect*, this paper presents a compressive self-powering approach that significantly enhances the powering/sensing range of our previously reported self-powered strain-sensor [1], [9]. The approach is illustrated in Fig. 2(b), where a high-gain piezoelectric transducer is first used to reach the powering-threshold V_{min} at low-levels of strain ε_{min}. Subsequently, the gain is progressively reduced such that the upper sensing-threshold V_{max} is reached at large-levels of strain ε_{max}. As we will show in section II, this type of compressive response can be achieved by connecting a non-linear resistive load at the output of the piezoelectric transducer. However, the compressive response also requires that the event detection circuits be precisely calibrated. In section III we propose to use a variant of our previously reported linear floating-gate injector circuit [10] to design precision event detectors and event loggers. In our previous work [1], [9] we had reported event loggers using a log-linear floating-gate injector circuit which had an operating range less than 100mV and a measured resolution of less than 6 bits. In comparison, the linear floating-gate injectors can achieve more than 13 bits of storage resolution over a 4V operating range, and is therefore well suited for event detection using the proposed compressive self-powering. In section IV, we present a system-on-chip solution that integrates programming and calibration circuitry with the event detection and logging circuits. We validate the functionality of the system using measured results from prototypes fabricated in a 0.5μm CMOS process and in section V we conclude the paper with some final remarks.

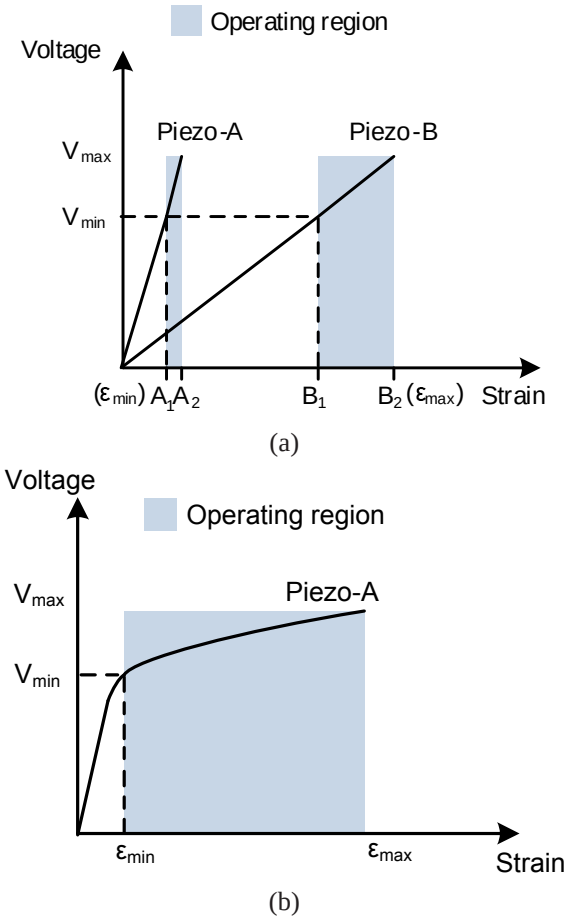

Fig. 2. Sensor Operating Region : (a) without any Compressive Gain; (b)with Compressive Gain.

II. Compressive Strain-powered Piezoelectric Sensor Circuit

Fig. 3 shows the implementation of the compressive self-powering front-end circuit connected to a piezoelectric transducer which is represented by its non-resonant (low-frequency) equivalent circuit model [12]. The capacitance C_p models the mechanical stiffness of the transducer and the voltage source V_{in} models the electrical signal transduced by strain variations. For a piezoelectric cantilever with dimensions $l \times w \times h$, the open-load voltage($v_{in}(t)$) generated across the transducer as a function of a perpendicular mechanical force $F(t)$ is given by [13]:

$$V_{in}(t) = \frac{F(t)g_{31}}{b} = S(t)Y^E h g_{31} = \frac{S(t)Y^E d_{31} h}{\varepsilon_p} \qquad (1)$$

where g_{31} and d_{31} are piezoelectric constants, $S(t)$ is the time-varying mechanical strain, Y^E is the short circuit elastic modulus and ε_p is the electrical permittivity of the transducer. R_L represents the load resistance, C_L the load capacitance and C_P represents the output capacitance of the transducer given by

$$C_p = \varepsilon \frac{w \times l}{h}. \qquad (2)$$

A resistive divider shown in Fig. 3 is used for implementing over-current and over-voltage protection circuits. Note that the values of R_1, R_2 and R_3 in the network are chosen according to the specifications of the required protection. For this implementation we have chosen R_1=R_2=1MΩ and $R_3 = 99M\Omega$. The full-wave rectifier is implemented using pMOS diodes whose bulk is driven by cross-coupled pMOS transistors, as shown in the inset. The bulk-driven topology as reported in [15], [14], [1] ensures that the bulk of the pMOS diode is always maintained at the highest (out of the source and drain voltages) potential. Diodes $D_{R1} - D_{R4}$ form a full-wave rectifier. The load at the output of the rectifier is a non-linear resistor(formed by diodes D_1-D_{20} and two nMOS N_1 and N_2) and the sensor integrated circuit (IC) denoted by the load capacitance C_L and load resistance R_L in Fig. 3.

The operational principle of the compressive powering circuit is as follows. At low levels of strain or low piezoelectric output voltage, the diode-chain D_1-D_{20} offers a high-resistance electrical path. As a result, most of the voltage drop occurs across R_3 and the load. As the strain-level and the piezoelectric output voltage increases, the electrical resistance offered by the diode-chain decreases non-linearly and majority of the voltage drop occurs across R_1 and R_2. The diode chains consist of three conduction paths formed by diodes chains D_1-D_{10}, D_{11}-D_{18} and D_{19}-D_{20}. Note that the voltage $V_x \approx V_{out}/10$ drives

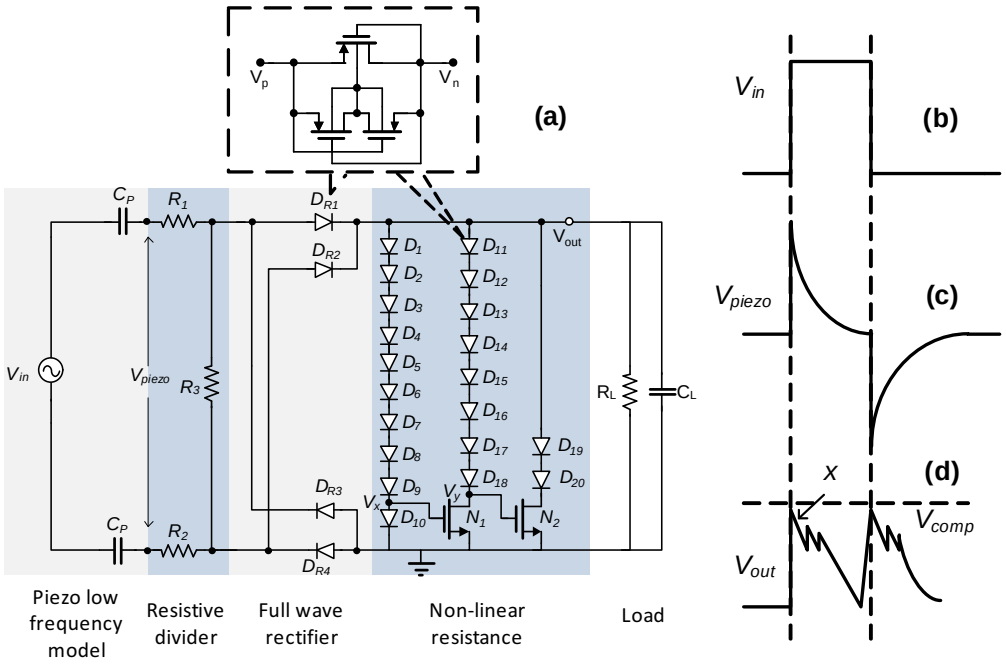

Fig. 3. (a) Schematic of the proposed non-linear compressive load connected to an equivalent circuit of a piezoelectric transducer; and the expected response when a strain-pulse (b) is applied; (c) corresponding output voltage of the piezoelectric transducer with no-load; and (d) output with the compressive load.

the gate of the nMOS transistor N_1. Thus, when $V_x < V_{th}$, with V_{th} being the threshold voltage of N_1, the diode chain D_{11}-D_{18} conducts negligible amount of current. Therefore, V_y follows $V_x \approx V_{out}/10$ which implies that the diode chains D_{11}-D_{18} and D_{19}-D_{20} simultaneously start conducting current. However, note that as the current through D_{11}-D_{18} increases the voltage V_y changes approximately as $V_y \approx V_{out}/5$. This makes N_2 turn ON faster which further draws more current from the node V_{out}. Fig. 3(b)-(d) shows a sketch of the transient response when the piezoelectric transducer is subjected to a mechanical impulse, modeled by the step change in the open-load voltage V_{in}. Fig. 3(c) shows the corresponding output voltage V_{piezo} when the full-bridge rectifier or the non-linear load is not connected. The transient response for V_{out} conforms to a transient response of a series R-C circuit and depicts the capacitive nature of a piezoelectric transducer. Fig. 3(d) shows the output voltage V_{out} when the non-linear resistor is connected. Region x in Fig. 3(d) corresponds to the instant when the diodes D_{19}-D_{20} start conducting, thus discharging the voltage V_{out}. However, when V_{out} reaches the threshold $V_{th}/5$, the transistors N_1 and N_2 are switched off, which leads to a jump in the voltage V_{out}. Because of the decoupling capacitor C_P there exist a zero at DC frequency and it can be shown that the magnitude of the peak output voltage V_{comp} is inversely proportional to the load resistance. Thus, when the magnitude of open-load voltage of the piezoelectric transducer increases (during high velocity impacts), reducing the load resistance would effectively result in reducing the output voltage, and thus lead to a compressive response.

Fig. 4 shows a simulation result where a sequence of mechanical impacts has been modeled as a train of impulses. The result shows V_{out} when the magnitude of the impulses (proportional to the velocity of the mechanical impact) is increased linearly. The response clearly shows that at low-levels of strain, V_{out} reaches the minimum threshold required to activate the sensor. Beyond the minimum threshold, V_{out} starts saturating which ensures that the maximum threshold level is not exceeded at high strain-levels.

III. Mechanical Impact Detection and Logging for Compressive Self-Powering

While numerous piezoelectric signatures could be used for detecting mechanical impact, in this paper, the occurrence of the event is signified when the magnitude of the piezoelectric output voltage exceeds a pre-defined threshold. The goal of the detection and logging circuit will then be to capture the statistics of this high-energy event (cumulative duration and

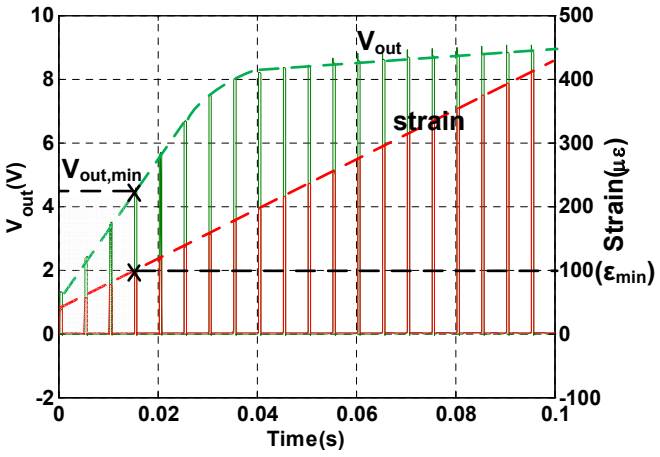

Fig. 4. Simulation result demonstrating a compressive response of the circuit shown in Fig. 3.

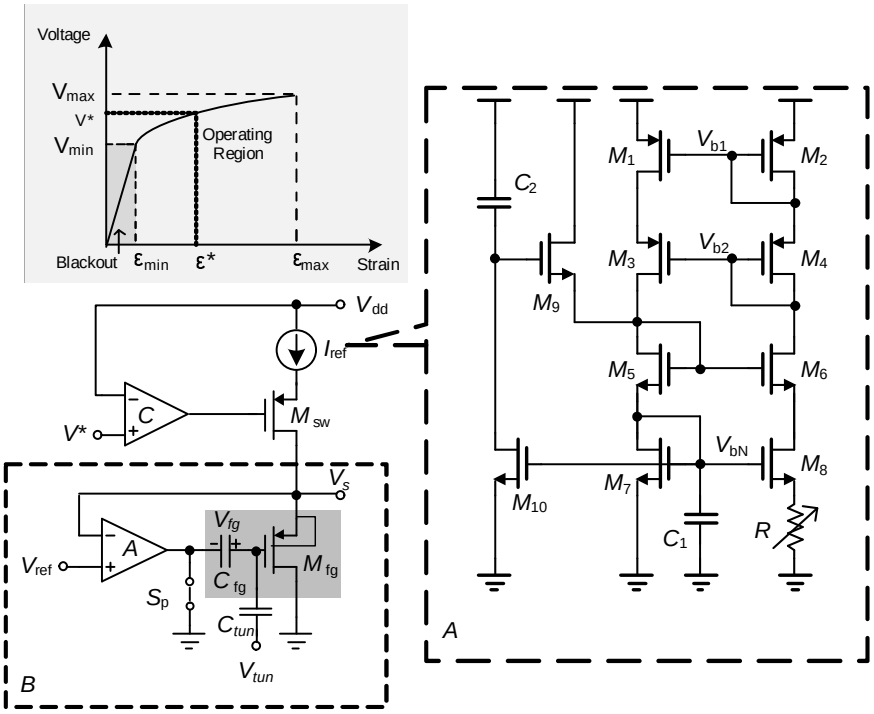

Fig. 5. Event detection and event counting using a linear floating-gate injector *B* driven by a constant current reference *A*.

cumulative event counts). Fig. 5 shows the schematic of a basic self-powered circuit that can be used to count and log the number of times the strain-level (proportional to the magnitude of the impact) exceeds a pre-determined threshold level ε^*. This corresponds to the number of times and the total duration for which the output of the comparator C is set low (or the pMOS transistor M_{sw} is turned ON). Note that the input voltage level of the comparator V^* is programmed according to the transfer function of the compressive self-powering front-end, as shown in Fig. 4. A linear floating-gate injector B shown in Fig. 5 accumulates the event-counts and stores the cumulative value on a non-volatile memory implemented by the floating-gate transistor M_{fg}. We briefly describe the operation of the linear floating-gate injector since the basic circuit has been extensively characterized in [10]. However, note that the use of linear floating-gate injectors for self-powered event counting and logging is reported for the first time in this paper.

A. Model of Linear Floating-gate Injectors

The basic architecture of the linear floating-gate injector is shown in Fig. 5 (inset B) and consists of a floating-gate transistor M_{fg} whose gate is electrically insulated by silicon-dioxide (hence the name "floating-gate"). Therefore, any electron injected onto the gate is retained for a long period of time (8 bits precision for 8 years) [16], [20]. Electrons are injected onto the floating-gate using an impact-ionized hot-electron injection (IHEI) process which involves applying $V_{\rm sd} > 4.2$V (in 0.5-μm CMOS process) across the source and the drain terminal. The large electric field near the drain of the pMOS transistor creates impact-ionized hot-electrons whose energy when exceeds the gate-oxide potential barrier ($\approx$3.2eV) can get injected onto the floating-gate. When the switch M_{sw} is ON, the reference current $I_{\rm ref}$ drives the source of M_{fg}. The opamp A forms a feedback network that ensures that $V_{\rm sd}$ is maintained at a constant potential. Thus, all voltage and current parameters (source current, gate, drain and source voltages) are held constant. This ensures that the injection current $I_{\rm inj}$ is constant.

If τ denotes the set of times when the switch M_{sw} is ON, then the decrease in floating-gate voltage $V_{\rm fg}$ is given by

$$\Delta V_{fg} = \frac{1}{C_T}\int_{t\in\tau} I_{inj}dt = \frac{I_{inj}}{C_T}\int_{t\in\tau} dt. \qquad (3)$$

C_T is the total floating-gate capacitance which includes the capacitance C_{fg}, tunneling capacitance and other parasitic capacitances associated with the floating node. The change in floating-gate voltage ΔV_{fg} could be measured by closing the switch $S_{\rm P}$ which breaks the feedback loop by shorting the other terminal of C_{fg} to ground. Because the source current $I_{\rm ref}$ is constant, $\Delta V_s = \Delta V_{fg}$ which is read out using a unity-gain buffer. Fig. 5 (inset A) shows the schematic of a standard supply independent current reference circuit (along with a capacitive start up circuit) which is used for generating the constant current $I_{\rm ref}$. Fig. 6 shows the measured response of the linear injector where the injector voltage linearly decreases with the number of times the switch M_{sw} is turned ON (programming cycles). Fig. 6 also shows that the slope of the injector can be varied by changing the voltage $V_{\rm ref}$. This attribute has been exploited in the next section for calibrating the mismatch related artifacts in the injectors.

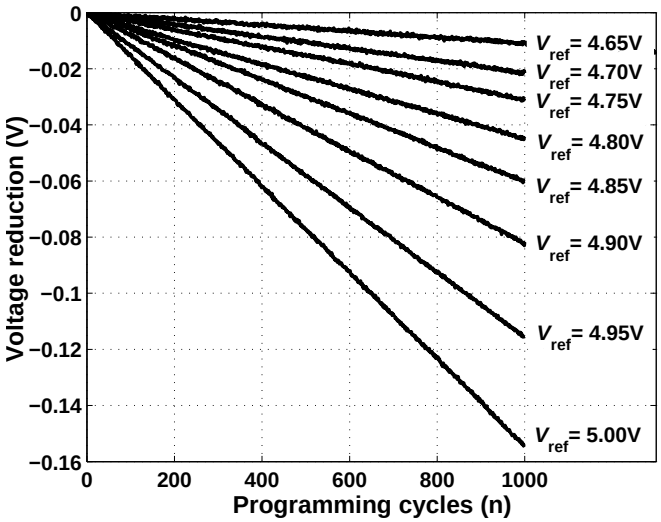

Fig. 6. Measured response of the linear injector when V_{ref} is varied.

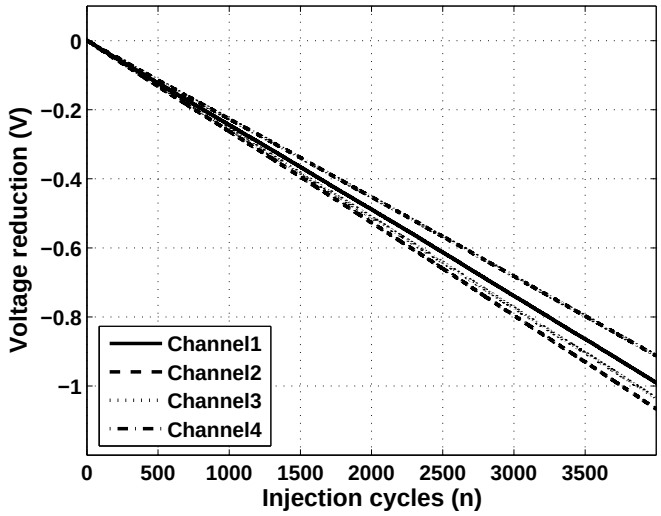

Fig. 7. Measured results showing gain mismatch between four injectors.

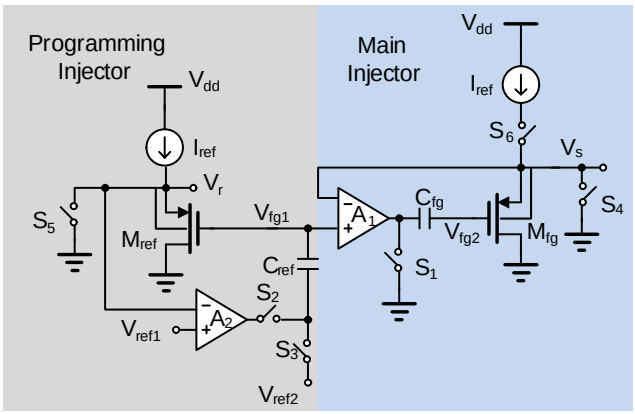

Fig. 8. Circuit for compensating the gain mismatch of a linear injector.

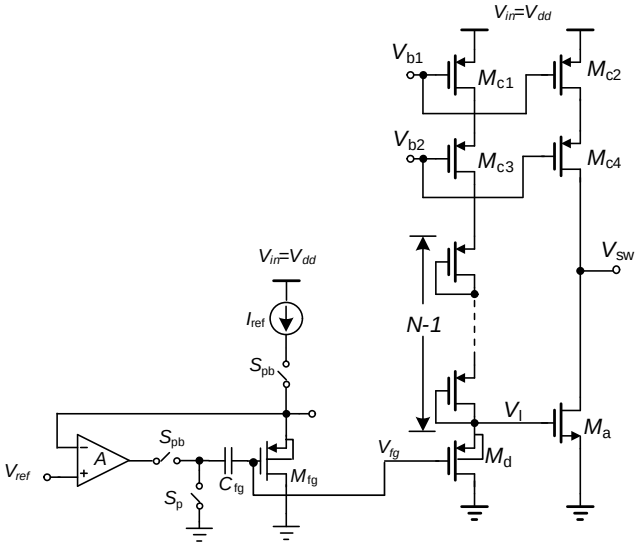

Fig. 9. Linear injector circuit for programming the comparator threshold.

B. Mismatch Compensation of the Linear Floating-gate Injectors

The key circuit element in the linear injector shown in Fig. 5 is the amplifier A which sets the source-to-drain voltage when the feedback is activated. Note that the injection current I_{inj} exhibits an exponential dependency with respect to the source-to-drain voltage and hence with respect to the amplifier offset voltage. Other factors that contribute towards the mismatch between the response of different linear injectors include the mismatch in reference currents I_{ref}, differences in hot-electron injection efficiency and the mismatch in floating-gate capacitance C_T. Fig. 7 shows injection results measured from different injectors clearly demonstrating mismatch in gains. This gain mismatch is problematic for the proposed compressive self-powering because of the limited comparator programming range. Fortunately, the effect of different mismatch contributors can be lumped together as an offset voltage mismatch between the feedback amplifier which can be effectively calibrated using floating-gate trimming techniques.

Fig. 8 shows an offset compensation technique that uses two linear injector circuits. Note that compensation of the linear injector could potentially be achieved using conventional floating-gate methods [17], [18]. However, the linear response of the linear injector significantly simplifies the compensation algorithm compared to other floating-gate programming approaches [19] which require repeated measure and injection cycles. In the circuit shown in Fig. 8, one of the injectors (referred as the programming injector) is used as a bias generator for programming the offset voltage V_{ref} of the main injector formed by the floating-gate transistor M_{fg}, amplifier A_1, control capacitor C_{fg} and the current source I_{ref}. When the switch S_1 is OFF the main injector is activated. The switch S_4 is a channel select switch which is turned ON when the main injector has to be de-activated (to prevent hot-electron injection through M_{fg}). This allows for selective programming and calibration of when multiple injectors are used in the sensor. When S_1 is ON, the voltage on the floating-gate V_{fg2} is read-out as V_s through the source follower formed by M_{fg}

and I_{ref}. The switch S_6 is turned on during the read-out and as well as during the hot-electron injection. The reference voltage of the amplifier A_1 is determined by the floating-gate voltage V_{fg1} that is programmed through another injector formed by M_{ref}, amplifier A_2 and reference current I_{ref}. Note that the amplifier A_1 internally uses cascoded structures to prevent hot-electron injection through the gate of the input transistor. The switch S_5 is used for de-activating the second injector after the gain mismatch has been compensated. During the self-powered operation of the sensor, the switch S_2 is OFF, S_5 is ON and the switch S_3 is connected to V_{ref2}. As a result the floating-gate reference voltage $V_{fg1} = C_{ref}/C_T.V_{ref2} + Q/C_T$, where Q is the total charge on the floating-node V_{fg1} and C_T is the total capacitance of the floating-node.

C. Coarse-fine Threshold Programming

The comparator C in Fig. 5 is implemented using the circuit shown in Fig. 9. Note that for self-powering, the comparator supply current, the comparator reference voltages and the comparator bias voltages has to be derived from the comparator input signal, therefore, conventional comparator topologies can not be directly used. M_{c1} and M_{c3} form a cascoded current source that feeds current into to a chain of (N-1) diode-connected PMOS. The bias voltages for the cascoded current source V_{b1} and V_{b2} are generated from a supply independent current reference shown in Fig. 5. The source of the pMOS M_d drives the input voltage V_l of a common-source amplifier formed by NMOS M_a and the cascoded current source M_{c2} and M_{c4}. As the input voltage V_{in} (which is the powering signal as well) increases, V_l increases and saturates at a voltage level that is determined by the cascoded current source (formed by M_{c1} and M_{c3}).

When V_l increases, the current through M_a increases and when the current becomes greater than the current through M_{c2} and M_{c4}, V_{sw} goes low which in turn triggers the injection switch M_{sw} in Fig. 5. The minimum input voltage V_{in} required to achieve this condition is determined by the number of pMOS diodes in the diode chain and the floating gate voltage V_{fg}. Thus, coarse programming of the switching threshold can be achieved by inserting different number of pMOS diodes, where as fine programming of the threshold can be achieved by tuning the value of V_{fg} using a linear injector as shown in Fig. 5. Programming of the linear injector formed by the floating-gate transistor M_{fg} and the amplifier A has already been described in the previous section and is omitted here.

Fig. 10 shows a simulated response of the circuit shown in Fig. 5 where an analog Verilog model of the floating-gate transistor has been used to incorporate the hot-electron injection equations [20] into SPICE simulation. For the simulation, the piezoelectric transducer parameters were chosen such that the transducer generates an open-load voltage greater than 5V at a strain of $100\mu\varepsilon$. The strain level was varied up to $10^4\mu\varepsilon$ and the compressive gain circuit ensures that V_{out} is limited to 13V. The threshold of five different comparators (Sw1-Sw5) were varied by inserting different number of pMOS diode elements in the circuit shown in Fig. 9. As shown in Fig. 10, each of the comparators span different levels of strain (labeled as Sw1-Sw5) in the compressive response. Within each of these regions, the threshold of the comparators can be fine-tuned by programming the linear injector in Fig. 9. Each of these comparator thresholds is illustrated by a vertical line which shows that the comparator output goes low when the input voltage level reaches a target threshold. The simulation results demonstrate that a 40dB of dynamic range can be effectively quantized using the coarse-fine threshold programming technique.

IV. System Architecture and Measurement Results

A. System Architecture

Fig. 11 shows the architecture of a system-on-chip that integrates the compressive powering front-end, the mismatch compensated linear injectors and an array of event detectors with programmable thresholds. The system architecture is divided into two main modules: (a) the self-powering module; and (b) the programming module. Even though the energy that can be scavenged from the piezoelectric transducer is sufficient for event detection, counting and non-volatile storage, the energy is not sufficient to program or configure the sensor. During the programming mode, an external supply $V_{ddD}(\sim 2V)$ activates the high-voltage charge-pumps which generate the supply voltage V_{dda} to drive the sensor and the read-out buffers. The high-voltage charge-pumps are also used for generating the tunneling voltage $V_{Tun}(\sim 16V)$ which is used for erasing the charge on the floating-gates of the linear injectors. A PoR(Power on Reset) generates the reset(RST) signal which is used to initialize the contents and state of all the digital registers and state-machines. A digital processor controls the hot-electron injection, tunneling and read-out through digital commands. The control commands(Cmd) are send to the processor as 24 bit words with a 12 bit preamble used to flag a valid data packet. All digital operations are synchronized using clock signals generated internally by a ring oscillator. An isolation diode similar to the one shown in Fig. 3 is used to separate the supply of the two modules such that the programming circuits do not load the piezoelectric transducer in the self-powering mode. The circuit level implementation of the charge-pump modules and the digital command and control has been reported in [11] and is omitted here for the sake of brevity. Next, we present measured results from a prototype system-on-chip (micrograph shown in Fig. 12) which has been fabricated in a 0.5-μm standard CMOS process.

B. Measurement Results

The first set of experiments is used for characterizing the DC response of the compressive front-end circuit shown in Fig. 3. A Keithley 2400 source meter was used to vary the voltage V_{piezo} and measure the current drawn by the non-linear resistor. Fig. 13(a) shows the I-V characteristics of the circuit and Fig. 13(b) shows the measured DC resistance as a function of the input voltage V_{piezo}. The measured results show that at lower magnitudes of the input voltage, the circuit emulates a large resistive load. This enables the output voltage to follow the input voltage and reach the minimum threshold required

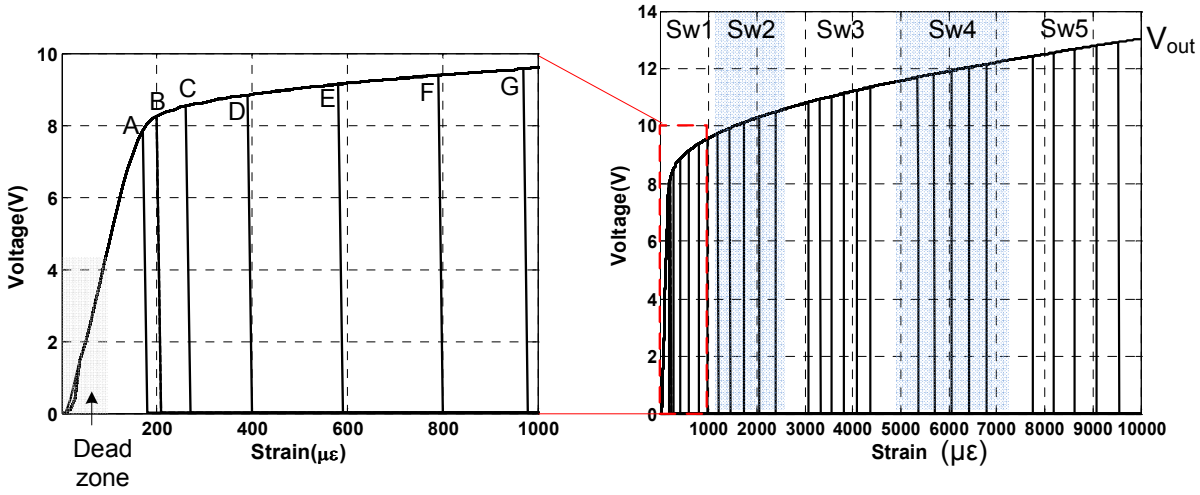

Fig. 10. Simulation result showing the compressive circuit allowing the sensor to operate from strain values of 100 to $10^4 \mu\varepsilon$. Detectors with five coarse thresholds have been programmed (fine-programming) to cover the input sensing range.

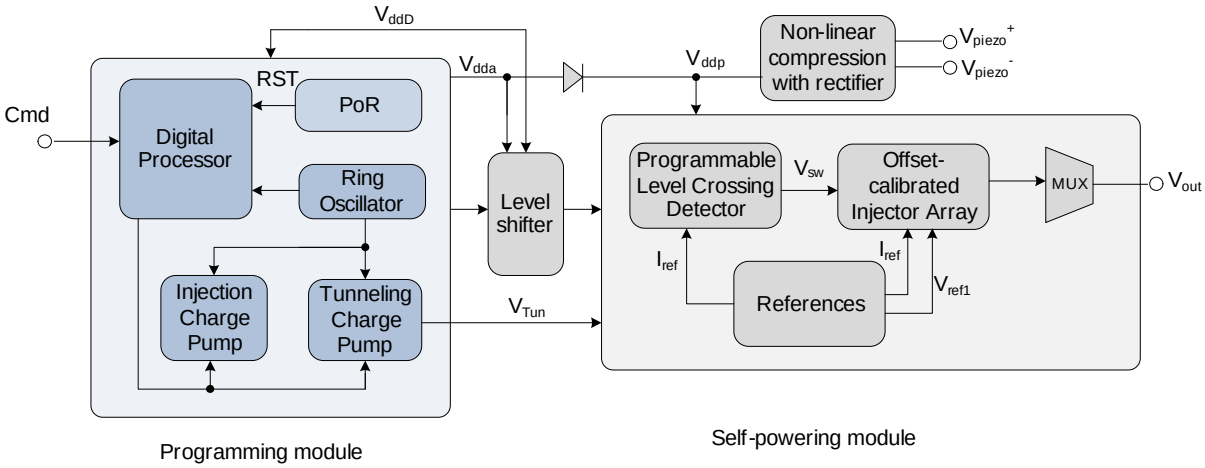

Fig. 11. System architecture of the system-on-chip integrating the self-powering and programming modules.

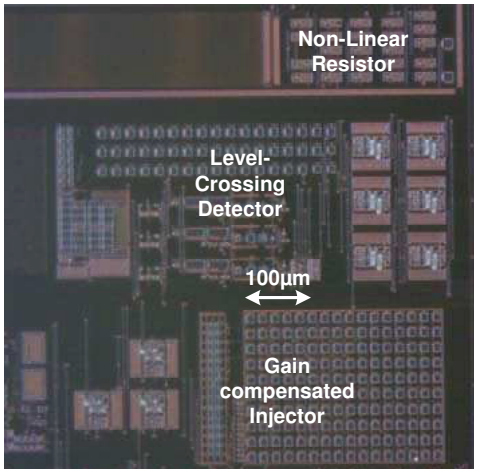

Fig. 12. Micrograph of the fabricated system-on-chip self-powered IC.

for powering the sensor. This is illustrated in Fig. 13(c), where the "dead-zone" signifies the region where the sensor is inactive. At higher magnitudes of the input voltage, the resistance rapidly drops which effectively saturates the output voltage as shown in Fig. 13(c). The measurement result is therefore consistent with the simulation result (zoomed in portion) shown in Fig. 10.

The next set of experiment validated the transient response of the compressive load by interfacing the fabricated prototype with a piezoelectric transducer. For this experiment, a PZT-5H transducer disk (diameter 2cm and thickness 10μm) was used as a sensor/transducer and was subjected to a low-energy mechanical impact (energy less than 1mJ) that can be easily generated without the use of specialized equipment. An oscilloscope (with 1MΩ probe setting) was used to measure the transient and Fig. 14(a) shows the open-load characteristic of the piezoelectric transducer. Note that for all the experiments the oscilloscope will act as a load (resistive and capacitive) to the transducer. As expected, the capacitive nature of transducer leads to a high-pass RC response as shown in the Fig. 14(a). Fig. 14(b) shows the measured output voltage (V_{out} in Fig. 3(a)) when the compressive load is connected

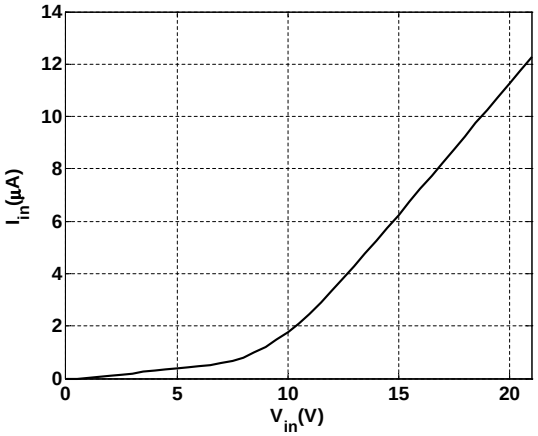

(a)

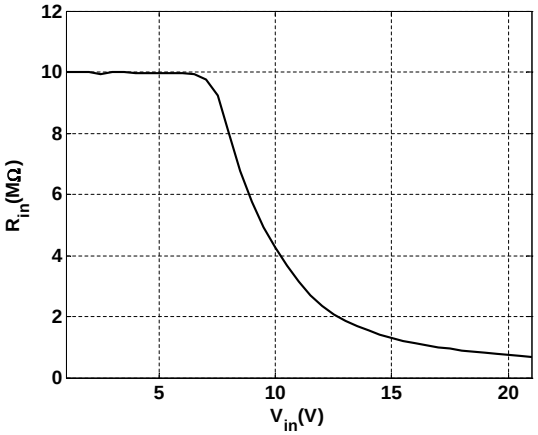

(b)

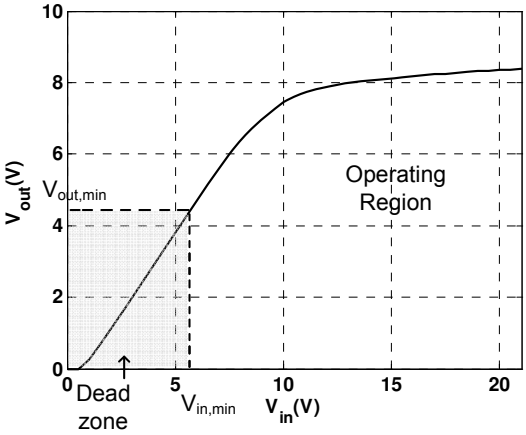

(c)

Fig. 13. Measured result for the Non-Linear compression circuit for a input sweep from 0 to 21V:(a) Input current; (b) Input resistance; (c) Output Voltage.

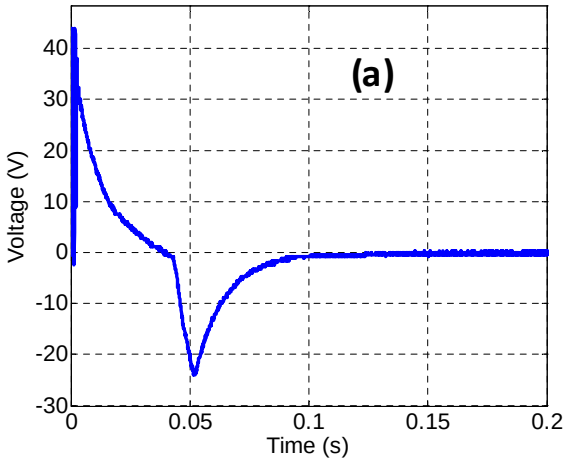

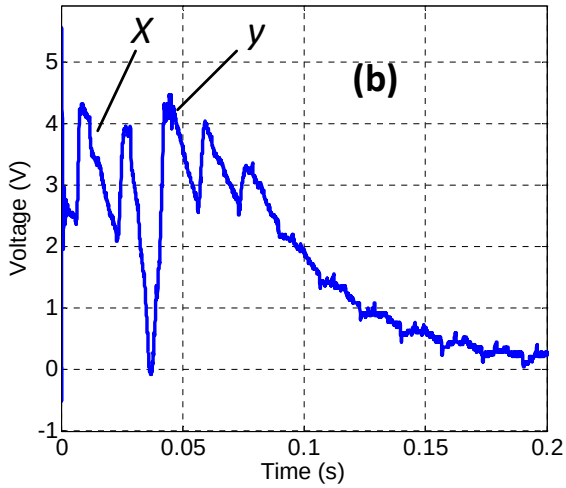

Fig. 14. Measured transient response when a sensor prototype is subjected a 1mJ mechanical impact: (a) output of the transducer with no load; and (b) output voltage with the compressive circuit.

to the transducer. The measured results validate the dynamic response of the non-linear resistance as was illustrated in Fig. 3(d). Region *x* in Fig. 14(b) corresponds to the condition when the output voltage $V_{out} > V_{th}/5$ and the nMOS transistors N_1 and N_2 (in Fig. 3(d)) are turned ON.

The next set of experiments validate the coarse-fine programming of the comparator circuit shown in Fig. 9. For each experimental run, the threshold of the linear floating-gate injector is calibrated to different values and the input voltage V_{dd} is increased linearly from 0 to 9V. Fig. 15 shows that the output of the comparator V_{sw} triggers (goes HIGH to LOW) at different threshold voltages. Note that for the calibration to be effective, the floating-gate voltage V_{fg} has to programmed to a negative voltage such that V_l (in Fig. 9) is less than the threshold voltage.

The next experiment demonstrates gain mismatch compensation of the linear injectors. During the compensation procedure, the programming injector (shown in Fig. 8) is calibrated till the measured injection rate reaches a pre-defined threshold. Fig. 16 shows the difference between the output voltages of three injectors before and after mismatch calibration. Run 1 and Run 3 show the difference in the injector response before calibration Run 2 corresponds to the result after calibration. The measured results clearly demonstrate that the injector gains can be effectively equalized using the circuit shown in Fig. 8.

The last set of experiments validated the performance of the system-on-chip using external command and control. The

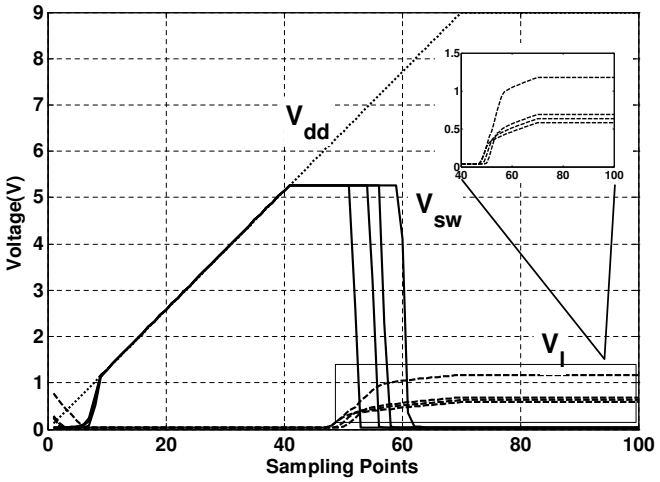

Fig. 15. Measurement results showing adjustment of comparator thresholds using the linear injector.

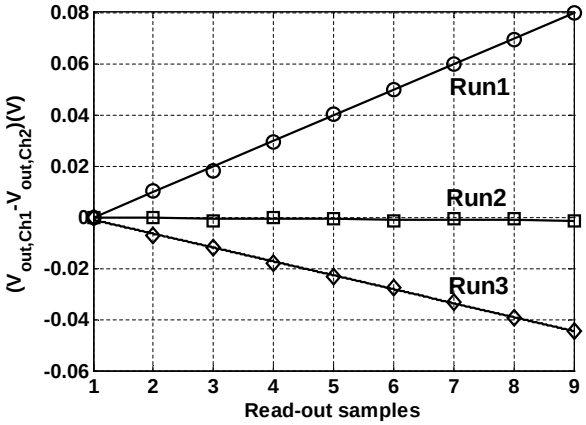

Fig. 16. Measured result of gain mismatch compensation circuit showing the difference in response between the three different injectors (Run 1 corresponds to difference between injector 1 and injector 2; Run 3 corresponds to the difference between the injector 1 and injector 3; and Run 2 corresponds to the difference between injector 1 and injector 2 after compensation).

schematic of the test setup used for this experiment is shown in Fig. 17. An initialization algorithm first erases the contents of the injectors using FN-tunneling and then programs the output V_s of each of the injectors using hot-electron injection within a reset range(2.5-3.5V). The control commands are invoked in MATLAB and is sent to the sensor through an Xilinx spartan-3 FPGA interface. The FPGA generates all the digital synchronization signals, details of which are provided in [1], [11]. Fig. 18(a) shows the measurement result, where the sensor is subjected to repeated mechanical impulses, erased and reconfigured. The change in the output of the injector for each mechanical event shows minimal deviation (less than 0.001V per mechanical event) across multiple runs demonstrating that the response of the sensor is stable after multiple injection and erase cycles. Fig. 18(b) shows the residue which characterizes the deviation in the measured response of the injector from an ideal linear response. Even though this result demonstrates 10 bits of linearity per run, by reducing the width of the pulses generated by the piezoelectric emulator, by reducing the gain

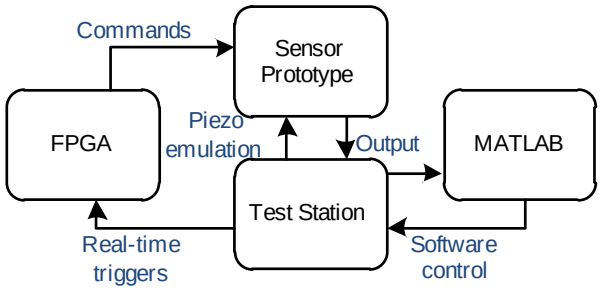

Fig. 17. Schematic of the test setup used for measuring the long-term sensor response.

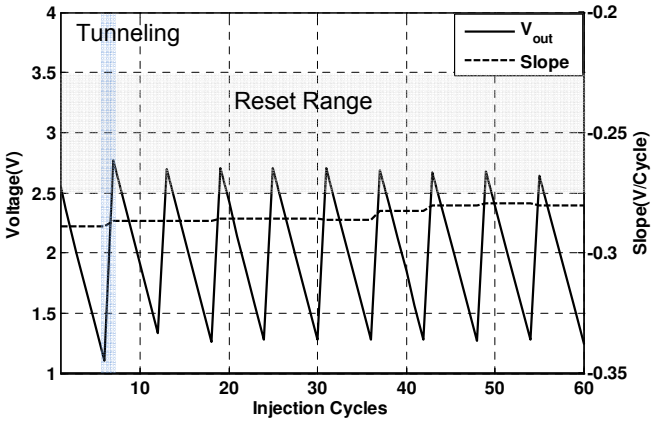

(a)

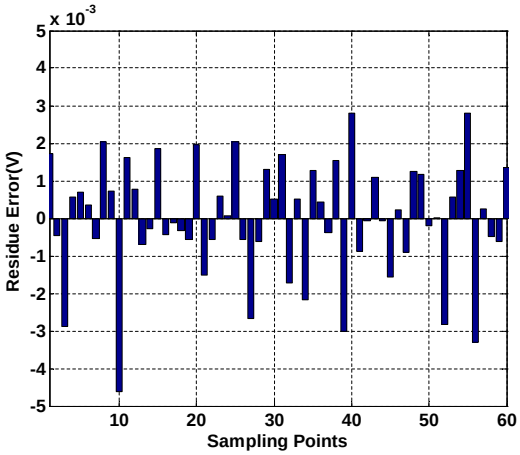

(b)

Fig. 18. Measurement result where the sensor was subjected to repeated injection cycles, each emulating a sequence of mechanical events; (a) showing event-counting followed by automatic erasure, programming and recalibration; (b) measured residue obtained after a linear regression on each event-counting region.

of the injector and by increasing the precision of the read-out buffer, up to 13-bits of linearity could potentially be achieved, which is the theoretical programming resolution that can be achieved using the linear injectors [10].

V. Conclusion

In this paper we described a novel compressive self-powering technique that overcomes the limited powering and sensing range of our previously reported piezo-floating-gate

sensors. The proposed technique uses a non-linear impedance circuit to dynamically load the output of a piezoelectric transducer and in the process reduce the magnitude of the output voltage at large levels of mechanical strain. We also presented a programmable mechanical event detection and counting circuit and an injector gain mismatch compensation circuit which enables the proposed sensor to effectively operate within the compressive powering and sensing range. The measurement results using a fabricated system-on-chip prototype validate the enhanced self-powering range of the sensor and demonstrate the programming and mismatch compensation of the parameters of interest. The proposed calibration technique could be also used to compensate for mismatch in the response of the piezoelectric transducer. The mismatch in the piezoelectric transducer properties (charge generated due to strain-variations) is determined by the dimensions of the transducer and by the quality of bonding between the transducer and the mechanical structure being monitored. However, it should be noted that ageing artifacts due to fatigue of piezoelectric transducers, temporal degradation of the piezoelectric bonding and mismatch due to temperature variations can not be compensated using the proposed static calibration technique.

REFERENCES

[1] C. Huang, S. Chakrabartty, "An Asynchronous Analog Self-powered Sensor-Data-Logger with a 13.56MHz RF Programming Interface," *IEEE Journal of Solid-State Circuits*, Feb 2012.

[2] R. Amirtharajah and A. P. Chandrakasan, "Self-powered signal processing using vibration-based power generation," *IEEE J. Solid-State Circuits*, vol. 33, no. 5, pp. 687-695, May 1998.

[3] Y. K. Ramadass and A. P. Chandrakasan, "A battery-less thermoelectric energy harvesting interface circuit with 35 mV startup voltage," *IEEE J. Solid-State Circuits*, vol. 46, no. 1, pp. 333-341, Jan. 2011.

[4] Y. L. Lee, J. Pan, R. Hathaway, and M. Barkey, "Fatigue testing and analysis: theory and practice," *ISBN-10: 0750677198*, 2004.

[5] S. Suresh, "Fatigue of materials," *2nd edition, Cambridge University Press*, ISBN-10: 0521578477, 1998.

[6] Dale S. Peerce and Vanessa S. Berg, "Bullet impact on steel and Kevlar/Steel Armor-Computer modelling and experimental data," *ASME Conf. Proc.*, 2004, 207 (2004).

[7] Keisuke Fujii, Eiichi Yasuda, Yasuhiro Tanabe, "Dynamic mechanical properties of polycrystalline graphites and a 2D-C/C composite by plate impact", *International Journal of Impact Engineering*, Volume 25, Issue 5, May 2001, Pages 473-491.

[8] Grujicic, M.; He, T.; Marvi, H.; Cheeseman, B. A.; Yen, C. F., " A comparative investigation of the use of laminate-level meso-scale and fracture-mechanics-enriched meso-scale composite-material models in ballistic-resistance analyses", *Journal of Materials Science*, vol. 45, issue 12, pp. 3136-3150.

[9] C. Huang, N. Lajnef and S. Chakrabartty, "Calibration and characterization of self-powered floating-gate usage monitor with single electron per second operational limit," *IEEE Transactions on Circuits and Systems I: Regular Papers*, vol. 57, no. 3, pp. 556-567, Mar 2010.

[10] C. Huang, P. Sarkar and S. Chakrabartty, " Rail-to-Rail, Linear Hot-Electron Injection Programming of Floating-Gate Voltage Bias Generators at 13-Bit Resolution," *IEEE Journal Of Solid-State Circuits*, vol.46, no:11, 2011.

[11] P. Sarkar, C. Huang and S. Chakrabartty, "An Ultra-linear Piezo-Floating-Gate Strain-Gauge for Self-powered Measurement of Quasi-static-strain", *IEEE Transactions on Biomedical Circuits and Systems(TBioCAS)*, under review.

[12] N.G Elvin and A.A Elvin, "A General Equivalent Circuit Model for Piezoelectric Generators," *Journal of Intelligent Systems and Structures*, May 2008.

[13] S. Chakrabartty and N. Lajnef, "Infrasonic Power-Harvesting and Nanowatt Selfpowered Sensors," *IEEE International Symposium on Circuits and Systems (ISCAS)*, pp.157-160, May 2009.

[14] N. Yan and H. Min, "A high efficiency all-PMOS charge pump for low-voltage operations," *Proc. IEEE Asian Solid-State Circuits Conference*, Hsinchu, Taiwan, Nov 2005, pp. 361364.

[15] R.Pelliconi, D.Iezzi et al, "Power Efficient Charge Pump in Deep Submicron Standard CMOS Technology," *IEEE Journal of Solid-state Circuits*, vol.38, No.6, June 2003.

[16] P. Hasler, "Foundations of learning in analog VLSI," *Ph.D. dissertation*, Dept. Comput. Neural Syst., California Inst. Technol., Pasadena, CA, 1997.

[17] Y. L. Wong, M. H. Cohen, and P. A. Abshire, "A floating-gate comparator with automatic offset adaptation for 10-bit data conversion," *IEEE Transactions on Circuits and Systems I: Regular Papers*, vol. 52, no. 7, pp. 13161326, Jul 2005.

[18] V. Srinivasan, G. J. Serrano, J. Gray, and P. Hasler, "A precision CMOS amplifier using floating-gate transistors for offset cancellation," *IEEE Journal of Solid-State Circuits*, vol. 42, no. 2, pp. 280291, Feb 2007.

[19] R. R. Harrison, J. A. Bragg, P. Hasler, B. A. Minch, and S. P. Deweerth, "A CMOS programmable analog memory-cell array using floating-gate circuits," *IEEE Transactions on Circuits and Systems II: Analog and Digital Signal Processing*, vol. 48, no. 1, pp. 411, Jan 2001.

[20] K. Rahimi, C. Diorio, C. Hernandez, and M. D. Brockhausen, " A simulation model for floating-gate MOS synapse transistors," *Proc. IEEE Int. Symp. Circuits Syst., Phoenix, AZ* , May 2002, pp. 532535.

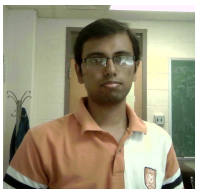

Pikul Sarkar Received the B.E degree in Electronics and Telecommunication Engineering from Jadavpur University, Kolkata, India in 2007 and an M.S. degree in Electrical and Computer Engineering from Michigan State University in 2012. Since August of 2012, he is with Cosmic circuits Inc., Bangalore, India. From 2007 to July 2010 he has worked as an analog design engineer in ST Microelectronics, India designing high speed serial link transmitters in 65nm, 45nm and 32nm technologies. His research interests include self powered sensors, piezoelectric energy scavenging, analog Computation, floating-gate circuits and systems, reconfigurable energy scavenging and data converters.

Shantanu Chakrabartty (SM'99-M'04-S'09) received his B.Tech degree from Indian Institute of Technology, Delhi in 1996, M.S. and Ph.D in Electrical Engineering from Johns Hopkins University, Baltimore, MD in 2002 and 2005 respectively.

He is currently an associate professor in the department of electrical and computer engineering at Michigan State University (MSU). From 1996-1999 he was with Qualcomm Incorporated, San Diego and during 2002 he was a visiting researcher at The University of Tokyo.

Dr. Chakrabartty's work covers different aspects of analog computing, in particular non-volatile circuits, and his current research interests include energy harvesting sensors and neuromorphic and hybrid circuits and systems. Dr. Chakrabartty was a Catalyst foundation fellow from 1999-2004 and is a recipient of National Science Foundation's CAREER award, University Teacher-Scholar Award from MSU and the 2012 Technology of the Year Award from MSU Technologies. Dr. Chakrabartty is a senior member of the IEEE and is currently serving as the associate editor for *IEEE Transactions of Biomedical Circuits and Systems*, associate editor for the *Advances in Artificial Neural Systems* journal and a review editor for *Frontiers of Neuromorphic Engineering* journal.